International Symposium
On Turbulence and Shear Flow
Phenomena (TSFP-8)
August 28 - 30, 2013 Poitiers, France

ROUGHNESS EFFECTS ON TURBULENT FLOW DOWNSTREAM OF A BACKWARD FACING STEP

Ebenezer E. Essel
Department of Mechanical and Manufacturing Engineering
University of Manitoba
Winnipeg, MB, Canada, R3T 5V6
essele@cc.umanitoba.ca

Godwin F. K. Tay
Department of Mechanical and Manufacturing Engineering
University of Manitoba
Winnipeg, MB, Canada, R3T 5V6
umtayg@cc.umanitoba.ca

Mark F. Tachie
Department of Mechanical and Manufacturing Engineering
University of Manitoba
Winnipeg, MB, Canada, R3T 5V6
Mark.Tachie@ad.umanitoba.ca

ABSTRACT

This study investigates the effects of surface roughness on turbulent shear flow downstream of a backward-facing step. Particle image velocimetry was used to conduct velocity measurements over two roughness elements and a reference smooth surface. In each test, the Reynolds number based on the step height and the centerline velocity was kept constant at 6750. The results show that roughness caused a marginal increase in the reattachment length. The distribution of the mean velocity, Reynolds stress, wall-normal transport of turbulent kinetic energy and spatial structures embodied in the two-point auto-correlation functions are independent of roughness in the recirculation region and immediately downstream of reattachment. Further downstream of reattachment, roughness reduced the streamwise mean velocity but increased the levels of the Reynolds stress, wall-normal transport of turbulent kinetic energy and the characteristic streamwise and wall-normal sizes of the spatial structures in the vicinity of the rough surface. Proper orthogonal decomposition is also used to reconstruct low-order representation of the flow field.

INTRODUCTION

Geometry-induced separated and reattached turbulent flows are encountered in diverse engineering applications. Because of their relative complexity (in comparison to canonical turbulent boundary layers), separated and reattached flows are also routinely used as acute test cases to assess the predictive capability of turbulence models. In view of their fundamental and practical importance, separated and reattached turbulent flows remain an important research topic. In fact many numerical and experimental studies have been performed over the past decades using geometries such as backward-facing step (BFS), forward-facing step, blunt plate and ribs to better understand the characteristics of separated and reattached turbulent flows over smooth surfaces (Bradshaw and Wong, 1972; Kostas et al., 2002). While the effects of Reynolds number and expansion ratio on the turbulence statistics in both the recirculation and recovery regions have been investigated thoroughly, our knowledge of surface roughness effects on separated and reattached flows is incomplete. Kim and Chung (1994) examined the flow field behind a BFS over k-type and d-type roughness elements, and observed that the k-type roughness increased the reattachment length by 3.4% in comparison with values obtained for the d-type and smooth surfaces. Surface roughness also reduced the mean velocity but enhanced the Reynolds normal stress in both the recirculation and recovery regions. More recently, Ren and Wu (2011) investigated the effect of roughness on turbulent flow over forward-facing steps. They observed that the mean velocity and Reynolds stresses within the recirculation region on the top surface of the step were strongly modified by the specific roughness topography. Ampadu-Mintah et al. (2012) studied the effects of roughness on open channel flow downstream of a BFS using wire-mesh, sand grains and a smooth surface. It was shown that the reattachment length and the mean velocity are independent of roughness. The turbulence intensities and Reynolds shear stress in the recirculation region were also independent of surface roughness.

The objective of this paper is to study roughness effects on separated and reattached turbulent flow downstream of a backward facing step. The measurements were performed over two types of sandpaper roughness and a reference smooth surface using a particle image velocimetry (PIV) technique. Proper orthogonal decomposition (POD) was employed to examine the dominant flow features in the flow field.

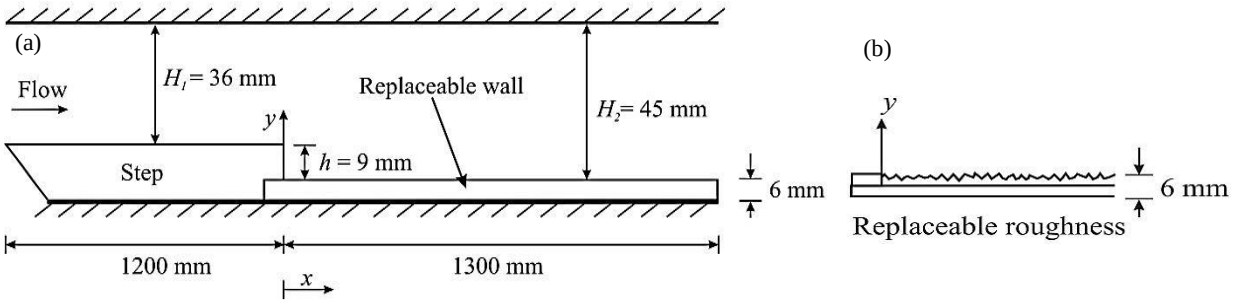

Figure 1. Sketch of (a) test section; (b) typical roughness element glued onto a replaceable plate

EXPERIMENTAL PROCEDURE

The experiments were conducted in a test channel that was screwed onto the bottom wall of a main recirculation water channel. The main channel was 2500 mm long, 200 mm wide and 200 mm deep. A sketch of the test channel and its relevant dimensions are shown in Fig. 1a. The internal width of the test channel was W = 183 mm. The BFS that was used to induce the flow separation has a nominal height, h = 9.0 mm and spans the first 1200 mm from the leading edge of the channel. The expansion ratio (H_2/H_1) and aspect ratio (W/h) are, respectively, 1.25 and 21. The walls of the main and test channels were made from transparent acrylic material to facilitate optical access. The roughness elements tested were sandpaper grit 36 (SP-36) and sandpaper grit 24 (SP-24). In addition to these two rough surfaces, measurements were also made on a reference smooth wall (SM). All the surfaces tested spanned 1300 mm long and were positioned immediately downstream of the step. As shown in Fig. 1b, the roughness elements were glued onto a replaceable plate.

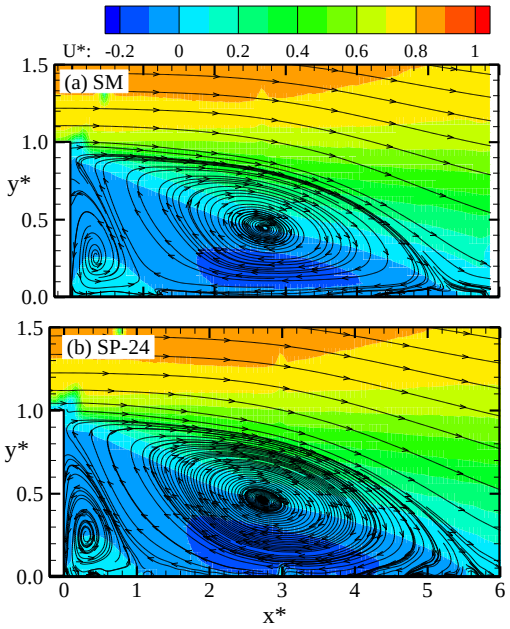

Figure 2. Contour plots of streamwise mean velocity over (a) smooth surface (SM), (b) sandpaper grit 24 (SP-24)

The combined thickness of the plate and the roughness elements was 6.0 mm, which is identical to the 6.0 mm acrylic plate used for the reference smooth surface.

The centerline mean velocity of the approach flow and Reynolds number based on the step height and the freestream velocity were kept constant at $U_e \approx 0.75$ m/s and Re_h = 6750, respectively, in each test. A PIV system was used to conduct detailed velocity measurements in the streamwise-wall-normal plane. The flow was seeded with 10 μm fluorescent tracer particles, and illuminated with a Nd:YAG double-pulsed laser that emits green light up to a maximum of 120 mJ/pulse at λ = 532 nm. A 12-bit CCD camera (with 2048 pixel × 2048 pixel array and 7.4 μm pixel pitch) fitted with an orange filter was used to image the flow field. Detailed measurements were made in an upstream plane centered at x^* (= x/h) = -7.5 to characterize the approach boundary layer, and also in 4 different planes that extend from x^* = -0.5 to x^* = 40, downstream of the BFS. A sample size of 6000 instantaneous image pairs was acquired in each plane to calculate the ensemble statistics. The interrogation area size was set to 32 pixels × 32 pixels with 50 % overlap in both streamwise and wall-normal directions. The spacing between adjacent velocity vectors was 0.05h, where h is the step height.

RESULTS AND DISCUSSIONS

Mean velocity and turbulence statistics

Contour plot of the streamwise mean velocity was obtained to visualize the mean flow pattern over each of the three surfaces tested. Since the plots in the separated and reattached regions were qualitatively similar over the 3 surfaces, only those over the smooth surface (SM) and the sandpaper grit 24 (SP-24) are shown in Fig. 2. The corresponding mean streamlines are overlaid on these plots to better reveal the flow pattern. In each case, both the primary recirculation zone and corner recirculation zone on the lower wall are well resolved. The mean reattachment point determined as the distance from the trailing edge of the step to the streamwise location where the mean separating streamline reattached onto the wall was found to be L_r/h = 5.4, 5.7 and 5.8 for tests SM, SP-36 and SP-24, respectively. The maximum backflow velocity was approximately 20% over the 3 surfaces.

The streamwise mean velocity (U), streamwise Reynolds normal stress (u^2) and the wall-normal transport of the turbulent kinetic energy, tke, (v^3+u^2v) were obtained

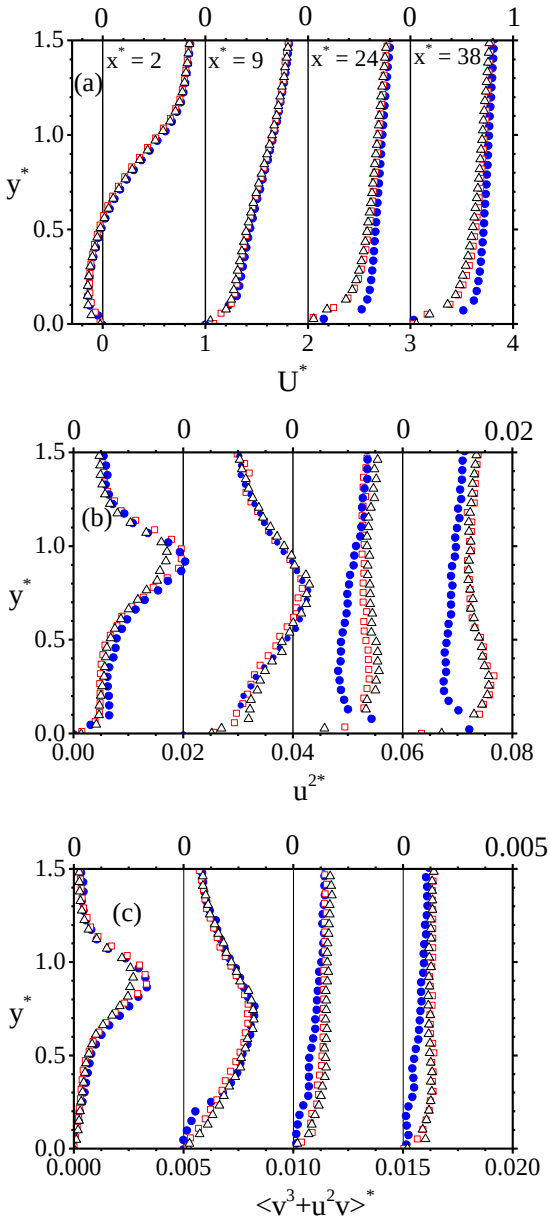

Figure 3. Distributions of (a) Streamwise mean velocity (b) streamwise Reynolds normal stress and (c) wall-normal transport of *tke* at selected streamwise location.

at selected streamwise locations to study the effects of surface roughness on the one-point turbulence statistics. The distributions of these statistics are plotted in Fig. 3. In each case, the local maximum mean velocity was used to normalize the data. Within the recirculation region (x^* = 2.7) and immediately downstream of reattachment (x^* = 9), the mean velocity, Reynolds stress and the wall-normal transport of *tke* do not reveal any dependence on surface roughness. Further downstream (x^* = 24 and 38), however, the impact of surface roughness on the flow dynamics is evident in the region adjacent to the wall. For example, the higher resistance caused by surface roughness reduced the mean velocity profiles over the rough surfaces considerably in comparison to the data over the smooth surface. Roughness also enhanced the levels of the Reynolds stress and wall-normal transport of *tke* in the near-wall region. The wall-normal extent across which roughness significantly modified the flow statistics, increases with increasing streamwise distance.

Two-points correleration

Two-point auto-correlation functions are also used to explore roughness effects on the statistical features of the coherent structure. The two-point spatial correlation function (R_{AB}) between any two arbitrary quantities $A(x, y)$ and $B(x, y)$ is defined as follows:

$$R_{AB}(x_{ref}+\Delta x, y_{ref}+\Delta y)=\frac{\langle A(x_{ref}, y_{ref})B(x_{ref}+\Delta x, y_{ref}+\Delta y)\rangle}{\langle \sigma_A(x_{ref}, y_{ref})\sigma_B(x_{ref}+\Delta x, y_{ref}+\Delta y)\rangle} \quad (1)$$

where (x_{ref}, y_{ref}) denotes the reference location, Δx and Δy are the spatial separations between A and B in the streamwise and wall-normal directions, respectively, and σ_A and σ_B are the root-mean-square values of A and B at (x_{ref}, y_{ref}) and ($x_{ref}+\Delta x$, $y_{ref}+\Delta y$), respectively. Typical one-dimensional profiles through the self-correlation point of the streamwise (R_{uu}) and wall-normal (R_{vv}) auto-correlation functions over SM and SP-24 at streamwise locations of x^* = 9 and x^* = 22 are shown in Fig. 4 and 5. These plots support the premise that the characteristic streamwise and wall-normal coherence and sizes of the spatial structure embodied in R_{uu} and R_{vv} over both surfaces increase with distance from the wall. The rapid decay of $R_{uu}(y)$ and $R_{vv}(y)$ for wall-normal distances below y_{ref} (particularly at y_{ref}^* = 0.25) is a manifestation of the reduced spatial size of the structures near the wall. Similar to the one-point turbulence statistics, it is observed that the characteristic streamwise and wall-normal sizes of the spatial structure embodied in R_{uu} and R_{vv} were independent of roughness in the region immediately downstream of reattachemnt (Fig. 4). Further downstream of reattachment (Fig. 5), surface roughness significantly increased the spatial coherence of the structure in the vicinity of the wall (i.e., at y_{ref}^* = 0.25). The effects of surface roughness at this y_{ref} location are stronger on the wall-normal than streamwise auto-correlation function.

Proper Orthogonal decomposition

Proper orthogonal decomposition (POD) is an unbiased statistical technique for identifying coherent structures in turbulent shear flows. The POD decomposes experimental or numerical data into series of modes, in which, the most energetic and hence the largest structures of the flow are captured in the first few modes. Because of the fast convergence of POD for the large scale structures, it is possible to isolate the large scales from the smaller scales, and to study the dynamic roles of the large scales on turbulence generation and transport. In this study, the POD analysis was implemented using the snapshot approach proposed by Sirovich (1987). In this method, each instantaneous PIV image is considered a snapshot of the flow field and the total number of snapshots is denoted by N. A detailed description of the implementation of snapshot POD analysis can be found in Shah and Tachie (2009). Due to space limitation, only the results obtained in the flow field immediately downstream of reattachment

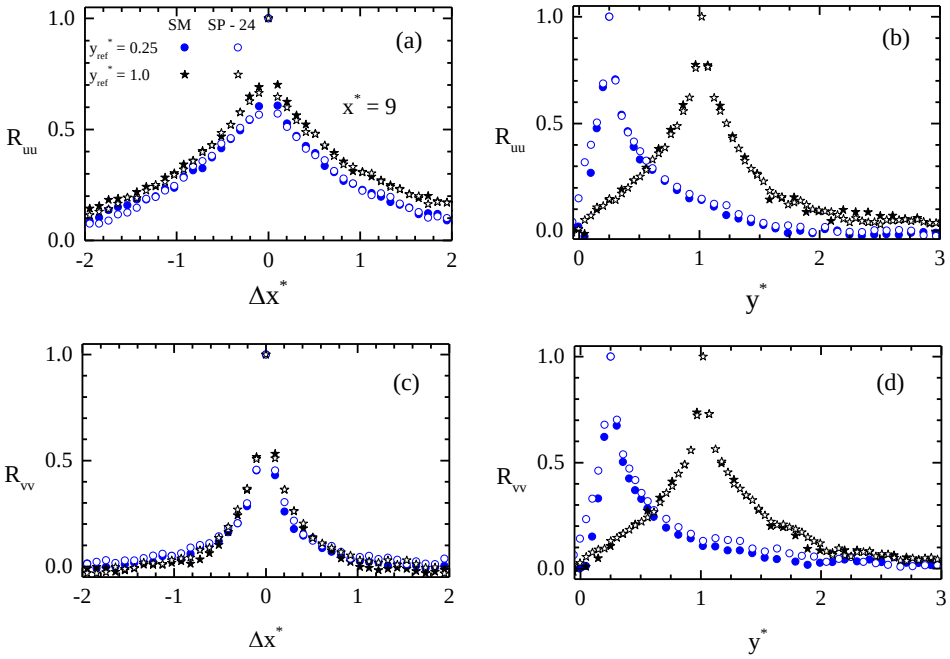

Figure 4. Profiles of two-point correlation functions at x* = 9 and various wall-normal reference (y_{ref}) locations.

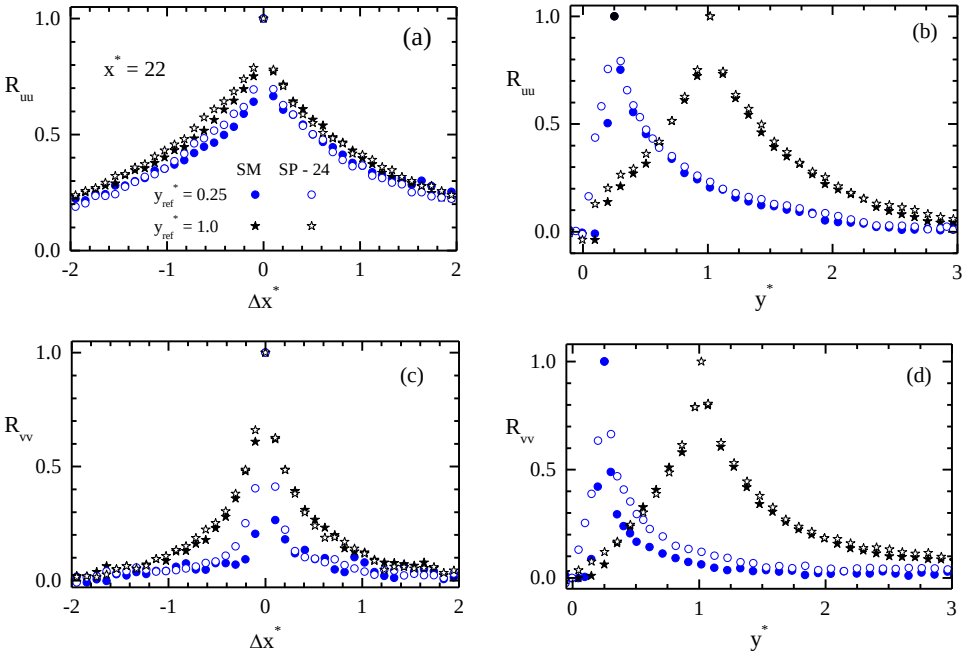

Figure 5. Profiles of two-point correlation functions at x* = 22 and various wall-normal reference (y_{ref}) locations.

(plane 2) over the smooth wall are presented. A convergence test was done to determine the number of snapshots required to adequately capture the energy content for a given mode. Table 1 shows the proportion of turbulent kinetic energy associated with the most dominant mode ($\lambda_1/\Sigma\lambda$) for an increasing number of snapshots. It is observed that variation in the value of $\lambda_1/\Sigma\lambda$ is negligible for $N \geq 500$. Thus, N = 6000 snapshots used in the present analysis is sufficient. The spectra of fractional and cumulative energy contributions of the first 50 modes are shown in Fig. 6. As expected, the fractional energy contribution of each mode decreased exponentially with increasing modes. After 30 modes, the energy content of each mode is less than 1%.

Table 1. Energy convergence for increasing number of snapshots (N) of the first mode, $\lambda_1^* = \lambda_1/\Sigma\lambda$ (%).

N	10	50	100	500	1000	4000	6000
λ_1^*	28.7	15.4	13.5	11.0	10.6	10.6	10.5

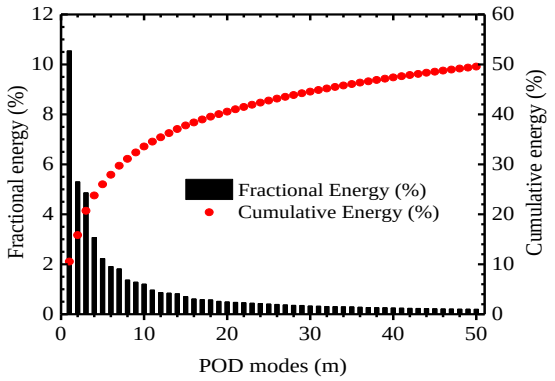

Figure 6. Distributions of the fractional and cumulative turbulent kinetic energy for the first 50 POD modes

It was observed from the cumulative energy distribution that 50% and 90% of the total energy was respectively captured using 52 and 2012 modes (not shown). A low order reconstruction of the instantaneous velocity field was performed to explore the dynamics of the energetic structures. From the reconstructed velocity field, contour plots of reconstructed turbulent kinetic energy (tke^*) and Reynolds shear stress ($-uv^*$) were obtained from the first few modes (1, 2, 3, 5 and 10) and the plots are shown in Fig. 7. The corresponding plots obtained from the ensemble-averaged PIV data are also shown in Fig. 7. The percentage cumulative *tke* contributions of the modes are shown on the contour plots of the tke^*. To reveal some features of the coherent structures embodied in mode 1, 2, 3, 5 and 10, eigenvectors are overlaid on the respective tke^* contour plots. These vector plots are representative of the spatial shapes of the coherent structures in the flow field. The vector plots reveal counter-rotating vortices. The contour plots of the reconstructed tke^* and $-uv^*$ are qualitatively similar in each of the modes. The plots also revealed changes in the intensity and spatial distribution of the dominant structures as the number of modes used in the reconstruction of these structures increases. In the first mode, for example, the energetic region and dominant structures, shown as high intensity peaks occur mid-way of the plane but shift downstream in the first 2 modes. The dominant structures in the first 3 and 5 modes are concentrated at multiple streamwise locations but by the first 10 modes, the contours begin to show the expected gradual decay of tke^* and $-uv^*$ observed in the ensemble-averaged PIV data. These distributions also suggest that as the number of modes increases, the reconstructed tke^* and $-uv^*$ gradually gain resemblance to the PIV data.

Conclusion

A high resolution particle image velocimetry technique was used to investigate roughness effects on the separated and reattached flow downstream of a backward facing step. Detailed velocity measurements were performed over two types of sandpaper roughness elements and a reference smooth surface. The results indicate that the reattachment length was marginally increased by roughness. Within the recirculation region and immediately downstream of reattachment the profiles of the mean velocity, Reynolds stress and wall-normal transport of *tke* were independent of surface roughness. However, further downstream, the higher resistance caused by surface roughness reduced the profiles of the mean velocity but enhanced the levels of the Reynolds stress and wall-normal transport of *tke* in the region adjacent to the rough surface. The effects of surface roughness on the characteristic streamwise and wall-normal sizes of the spatial structure embodied in R_{uu} and R_{vv} were not significant in the early recovery region but further downstream of reattachment, roughness increased the characteristic sizes of these spatial structures. Also, spatial structure embodied in R_{uu} and R_{vv} increased with distance from the wall. Proper orthogonal decompostion revealed distinct changes in the intensity and spatial distribution of the dominant structures as the number of modes used in the low order reconstruction of these structures increases.

Acknowledgements

The authors acknowledge the support of this work by the Natural Sciences and Engineering Research Council of Canada.

References

Bradshaw P. and Wong F. Y. F., 1972, "The Reattachment and Relaxation of a Turbulent Shear Layer" *Journal of Fluid Mechanics*, Vol. 52, pp. 113-135.

Kostas J., Soria J., and Chong M.S., 2002, "Particle Image Velocimetry Measurements of a Backward-Facing Step Flow", *Experiments in Fluids*, Vol. 33, pp. 838–853.

Ren H. and Wu Y., 2011, "Turbulent boundary layers over smooth and rough forward-facing steps," *Physics of Fluids*, Vol. 23, 045102, pp. 1-17.

Kim B. N. and Chung M. K., 2009, "Experimental study of Roughness effects on the separated flow over a Backward-facing step," *AIAA Journal*, Vol. 33, no. 1, pp. 159-161.

Ampadu-Mintah A. A., Tachie M. F., Agelin-Chaab M., 2012, "Roughness effects on separated and reattached open channel turbulent flow", *Turbulence, Heat and Mass Transfer 7*, Palermo, Sicily, Italy, Sept. 24-27.

Sirovich L., 1987, "Turbulence and the Dynamics of Coherent Structures, Part 1: Coherent Structures", *Quarterly Journal of Applied Mathematics*, Vol. 45, pp. 561 - 571.

Shah M. K. and Tachie M. F., 2009, Proper Orthogonal Decomposition Analysis of Separated and Reattached Pressure Gradient Flows, *AIAA Journal*, Vol. 47, no. 11, pp. 2616-2631

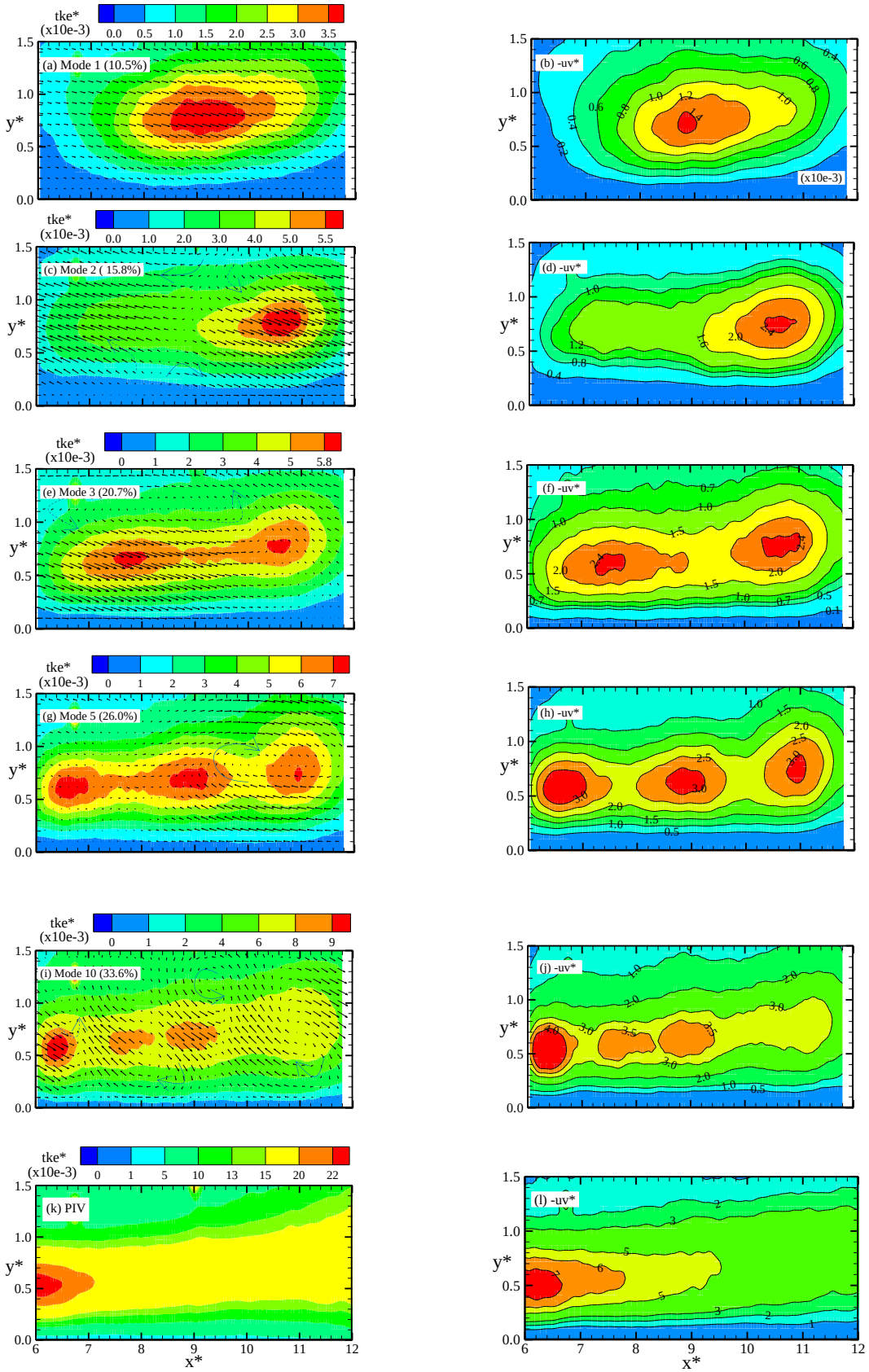

Figure 7. Contour plots of reconstructed turbulent kinetic energy and Reynolds shear stress